THE JOURNAL OF PHYSICAL CHEMISTRY B

 VOLUME 107, NUMBER 5, FEBRUARY 6, 2003

ARTICLES

Effect of Yb^{3+} Codoping on the Upconversion Emission in Nanocrystalline $Y_2O_3:Er^{3+}$

Fiorenzo Vetrone,[†] J. Christopher Boyer,[†] John A. Capobianco,*[,†] Adolfo Speghini,[‡] and Marco Bettinelli[‡]

Department of Chemistry and Biochemistry, Concordia University, 1455 de Maisonneuve Blvd. W, Montreal, QC, H3G-1M8 Canada, and Dipartimento Scientifico e Tecnologico, Università di Verona, and INSTM, UdR Verona, Ca' Vignal, Strada Le Grazie 15, I-37134 Verona, Italy

Received: August 12, 2002; In Final Form: November 12, 2002

The Stokes emission of nanocrystalline and bulk $Y_2O_3:Er^{3+}$, Yb^{3+} following 488 nm were reported. Two nanocrystalline samples were studied, one produced via propellant synthesis and the other via wet synthesis. Green, red, and NIR emission from the Er^{3+} ion was observed in both bulk and nanocrystalline samples. Emission from the $^2F_{5/2} \rightarrow {}^2F_{7/2}$ Yb^{3+} transition was also observed in the bulk and nanocrystalline samples following 488 nm excitation, thereby signifying the presence of an energy transfer process from Er^{3+} to Yb^{3+}. The peaks attributed to Yb^{3+} emission were much less intense in the nanocrystalline material, indicating that the energy transfer process occurs less readily in this material because of the inherent high phonon energies from the adsorbed CO_2 and H_2O on their surface. Following excitation with 978 nm, green and red anti-Stokes luminescence was evidenced in the samples under investigation. An enhancement of the red emission is observed in both bulk and nanocrystalline samples, although to a much greater degree in nanocrystalline $Y_2O_3:Er^{3+}$, Yb^{3+}. The enhancement of the red emission was shown to occur due to an ion-pair process of the form: $(^4F_{7/2}, {}^4I_{11/2}) \rightarrow (^4F_{9/2}, {}^4F_{9/2})$, which directly populates the $^4F_{9/2}$ state. However, this process cannot account for the drastic difference in the magnitude of the red enhancement between bulk and nanocrystalline samples. A phonon-assisted energy transfer process was found to be operative, which also populates the $^4F_{9/2}$ state. This process occurs more readily in the nanocrystalline material as the large vibrational quanta from the adsorbed carbonate and hydroxyl ions can easily bridge the mismatch in energy.

Introduction

Recently, considerable attention has been given to trivalent rare earth (RE^{3+}) doped phosphors with particle sizes in the nanometer regime.[1−4] The bulk of the research has focused primarily on their Stokes luminescence properties, studying the emission of radiation at an energy lower than that of the exciting wavelengths. The interest stems from the remarkable particle-size-dependent phenomena that can be exhibited by these nano-sized phosphors. For many of these studies, $Y_2O_3:RE^{3+}$ has been the material of choice owing to its favorable physical properties and ease of synthesis in the nanometer regime. In particular, the intensity of the rare earth luminescence[5] and lifetime of the excited states,[6] have been shown to be dependent on the size of the yttria particles. In contrast however, much fewer works have appeared on upconversion nanocrystalline phosphors, which provide the emission of radiation at higher energy than the excitation wavelength. The tripositive erbium ion is particularly suitable when it comes to upconversion. This is because it possesses a favorable electronic energy level scheme with equally spaced long-lived excited states. The efficiency of the upconversion depends on the spatial distribution of the dopant

* Corresponding author. Telephone: +1-514-848-3350. Fax: +1-514-848-2868. E-mail: capo@vax2.concordia.ca.
[†] Concordia University.
[‡] Università di Verona.

10.1021/jp0218692 CCC: $25.00
Published on Web 01/11/2003

ions. Thus, increasing the dopant concentration or choosing a host lattice whose structure enhances the formation of complexes of associated ions will result in an increased upconversion efficiency.[7]

We have studied the upconversion properties of nanocrystalline Y_2O_3:Er^{3+} in which the intensities of the upconverted emission were enhanced by increasing the Er^{3+} content in the crystal.[8] However, this was successful only to a certain extent and cannot be considered as a viable solution to increasing the upconversion luminescence because, at higher dopant concentrations, cross-relaxation between Er^{3+} ions quenches the green $^2H_{11/2}$, $^4S_{3/2} \rightarrow {}^4I_{15/2}$ transition, thereby decreasing the effect of the increased concentration. The Er^{3+} ion has a relatively low absorption cross-section for the transitions in the near-infrared (NIR) region around 1000 nm.[9] On the other hand, the Yb^{3+} ion exhibits a much larger absorption cross-section in this region and thus, codoping with Yb^{3+} has proven to be a successful alternative for the upconversion process. In fact, there is a large spectral overlap between the $^2F_{5/2} \rightarrow {}^2F_{7/2}$ Yb^{3+} NIR emission and the $^4I_{11/2} \leftarrow {}^4I_{15/2}$ Er^{3+} absorption bands, which results in an efficient energy transfer. The efficiency of this process depends on the energy matching between the energy of the transfer process and the energy gap between the levels of the Yb^{3+} and Er^{3+} ions.[10] When the matching is good, the transfer will take place resonantly with a high efficiency. If the matching is imperfect, the transfer still takes place but with a much lower efficiency. The simultaneous absorption or emission of phonons, which can bridge the energy mismatch, accompanies this nonresonant process.

In this paper, we study the effects on the upconversion properties of nanocrystalline Y_2O_3:Er^{3+} prepared via two synthesis routes following codoping with Yb^{3+} ions. The results are compared to the results obtained for an identically doped Y_2O_3:Er^{3+}, Yb^{3+} bulk sample.

Experimental Section

Sample Preparation. Codoped Er^{3+} and Yb^{3+} nanosized Y_2O_3 crystals of composition $Y_{1.96}Er_{0.02}Yb_{0.02}O_3$ were prepared utilizing two different synthesis routes. One nanocrystalline sample was prepared using a solution combustion synthesis procedure (propellant synthesis).[11,12] The propellant synthesis reaction involved an aqueous solution containing glycine, $Y(NO_3)_3$, $Er(NO_3)_3$, and $Yb(NO_3)_3$. The glycine serves as fuel for the propellant reaction, being oxidized by the nitrate ions. The synthesis reaction is

$$6M(NO_3)_3 + 10NH_2CH_2COOH + 18O_2 \rightarrow 3M_2O_3 + 5N_2 + 18NO_2 + 20CO_2 + 25H_2O$$

where M = Y, Er, and Yb. A glycine-to-metal nitrate molar ratio of 1.2:1 was employed to prepare the precursor solution. After the combustion, the powder was fired for 1 h at 500 °C to decompose the residual nitrate ions.

A different nanocrystalline sample was prepared using a controlled hydrolysis procedure (wet synthesis).[13] This method calls for the reaction of an alcoholic solution containing $Y(NO_3)_3$ and $Ln(NO_3)_3$ (Ln = Er and Yb) with a basic solution of a surface modifier (β-alanine + Tween 80 in a 1:1 weight ratio) at pH > 10 (ammonia solution).[14] The two solutions were mixed and the obtained gel was centrifuged for 1 h at a speed of 3000 rpm. After removing the aqueous solution, the powder was dried at 70 °C for 24 h and then heat treated in a muffle furnace for 12 h at 500 °C.

A detailed investigation using wide-angle X-ray scattering (WAXS) was undertaken to determine the average size of the Y_2O_3 crystallites obtained by the procedures described above.[14,15] The WAXS patterns for the nanocrystalline material obtained by the propellant synthesis indicated that the crystalline domains preserve the crystallographic structure of yttria (cubic system; space group *Ia*3) and that the average radius of the crystallites is about 20 nm. Similarly, WAXS also showed that the samples prepared by the wet synthesis have the same cubic structure with nanocrystallites on the order of approximately 10 nm. It is interesting that despite the very different morphology and nanostructure, the diffractograms of the samples prepared by the propellant and wet techniques are almost identical.

For comparative purposes, a bulk $Y_{1.96}Er_{0.02}Yb_{0.02}O_3$ sample was prepared by intimately mixing Y_2O_3 (Aldrich, 99.99%), Er_2O_3 and Yb_2O_3 (Aldrich, 99.99+ %), pressing the powders into pellets under 10 tons of pressure and firing them in air. Several heat treatments were attempted, but the optimum homogeneity (as checked by SEM) was obtained when the sample was fired at 1500 °C for 48 h. Spectroscopic measurements were carried out on a sample, which had undergone this heat treatment. It should be noted that the size of the particles in the bulk sample is at least 10 times larger than either one of the nanocrystalline samples.

All yttria samples were kept in air without any further precaution.

Infrared Reflectance Spectroscopy. The diffuse reflectance spectrum in the medium infrared (MIR) region was measured at room temperature using a Nicolet Magna 760 FTIR spectrometer using an aluminated mirror as a reference.

Stokes and Anti-Stokes Emission. Stokes emission spectra were obtained by exciting the bulk and nanocrystalline material at 488 nm using a Coherent Sabre Innova, 20 W argon ion laser. Anti-Stokes emission spectra were obtained with 978 nm (400 mW) using a Spectra-Physics Model 3900 titanium sapphire laser pumped by the 514.5 nm line of a Coherent Sabre Innova argon ion laser and with 1064 nm pulses from a Lumonics HY 400 Q-switched Nd:YAG laser (pulse duration ~10 ns, 400 mJ). The excitation light was focused (12 cm focal length) to a spot size of approximately 0.25 mm. The visible emissions were collected using a Jarrell-Ash 1 meter Czerny-Turner double monochromator and dispersed with a thermoelectrically cooled Hamamatsu R943-02 photomultiplier tube. A preamplifier, model SR440 Stanford Research Systems, processed the photomultiplier signals and a gated photon counter model SR400 Stanford Research Systems data acquisition system was used as an interface between the computer and the spectroscopic hardware. The signal was recorded under computer control using the Stanford Research Systems SR465 software data acquisition/analyzer system.

The near-infrared emission spectra were recorded in the region 900−1800 nm using a Jarrell-Ash 3/4-m Czerny-Turner single monochromator and the signal was detected by a liquid nitrogen-cooled Northcoast EO-817P germanium detector connected to a computer-controlled Stanford Research Systems SR510 lock-in amplifier.

Results and Discussion

The sesquioxide Y_2O_3 crystallizes in the cubic bixbyite structure with space group *Ia*3 (T_h^7).[16,17] In this lattice, the trivalent rare earth impurities have two distinct sites available for which to substitute the Y^{3+} cation without charge compensation. The two different sites, each six coordinate, possess C_2 and C_{3i} point-group symmetry.[18] The Y^{3+} ions are accommodated in 32 sites in the unit cell; 24 sites with point group symmetry C_2 and 8 sites with C_{3i} symmetry can be occupied by the RE^{3+} ions. However, the selection rules dictate that

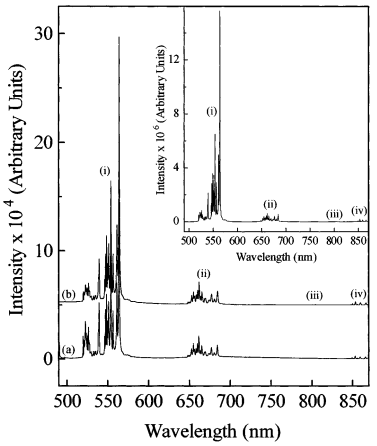

Figure 1. Room temperature Stokes luminescence of nanocrystalline $Y_2O_3:Er^{3+}$, Yb^{3+} prepared via (a) propellant and (b) wet synthetic routes following excitation with 488 nm. Inset: room-temperature Stokes luminescence of bulk $Y_2O_3:Er^{3+}$, Yb^{3+}: (i) $^2H_{11/2}$, $^4S_{3/2} \rightarrow {}^4I_{15/2}$; (ii) $^4F_{9/2} \rightarrow {}^4I_{15/2}$; (iii) $^4I_{9/2} \rightarrow {}^4I_{15/2}$; (iv) $^4S_{3/2} \rightarrow {}^4I_{13/2}$.

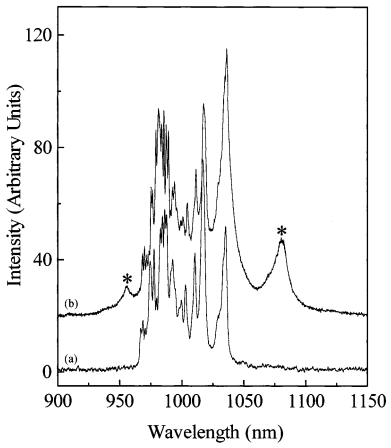

Figure 2. Near-infrared Stokes luminescence of the $^4I_{11/2} \rightarrow {}^4I_{15/2}$ transition in bulk (a) $Y_2O_3:Er^{3+}$ and (b) $Y_2O_3:Er^{3+}$, Yb^{3+} following excitation with 488 nm. Emission from the Yb^{3+} $^2F_{5/2} \rightarrow {}^2F_{7/2}$ transition denoted with an asterisk (*).

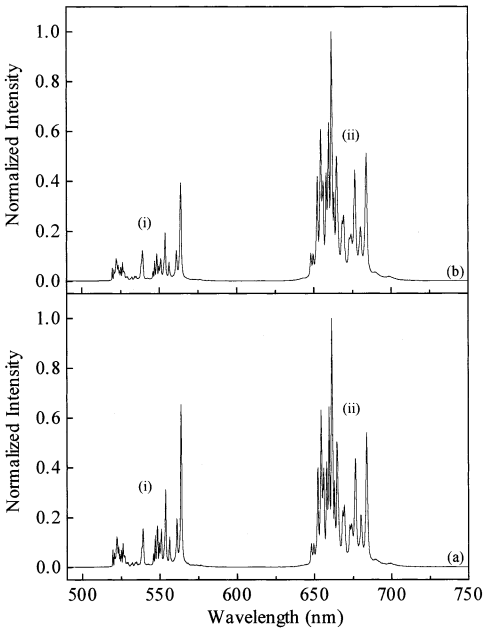

Figure 3. Room temperature anti-Stokes luminescence of nanocrystalline $Y_2O_3:Er^{3+}$, Yb^{3+} prepared via (a) propellant and (b) wet synthetic routes following excitation with 978 nm: (i) $^2H_{11/2}$, $^4S_{3/2} \rightarrow {}^4I_{15/2}$; (ii) $^4F_{9/2} \rightarrow {}^4I_{15/2}$

electric dipole transitions are forbidden for the rare earth dopant ions in the C_{3i} sites due to its center of inversion. Therefore, it is tacitly assumed throughout this paper that the observed f-f spectra are attributed to Er^{3+} ions in sites of C_2 symmetry.

Stokes Luminescence. The room-temperature emission spectra for the nanocrystalline $Y_2O_3:Er^{3+}$, Yb^{3+} samples produced by both the propellant and wet synthesis techniques in the 500−870 nm region and following 488 nm excitation, are shown in Figure 1. The spectra exhibit four distinct emission bands corresponding to the radiative decay from some excited states of the erbium ion. Green emission was observed between 500 and 580 nm corresponding to the thermalized $^2H_{11/2}$, $^4S_{3/2} \rightarrow {}^4I_{15/2}$ transition. Red emission was observed between 640 and 690 nm corresponding to the $^4F_{9/2} \rightarrow {}^4I_{15/2}$ transition. NIR emission was observed between 785 and 825 nm corresponding to the $^4I_{9/2} \rightarrow {}^4I_{15/2}$ transition and between 840 and 870 nm corresponding to the $^4S_{3/2} \rightarrow {}^4I_{13/2}$ transition.

Figure 1 (inset) presents the emission spectra for the bulk $Y_2O_3:Er^{3+}$, Yb^{3+} sample in the same spectral region as the nanocrystalline samples. Similar to the nano material, emission from the $^2H_{11/2}$, $^4S_{3/2} \rightarrow {}^4I_{15/2}$ transition was observed between 500 and 580 nm. Red emission was observed between 640 and 690 nm corresponding to the $^4F_{9/2} \rightarrow {}^4I_{15/2}$ transition. NIR emission was observed between 785 and 825 nm corresponding to the $^4I_{9/2} \rightarrow {}^4I_{15/2}$ transition and between 840 and 870 nm corresponding to the $^4S_{3/2} \rightarrow {}^4I_{13/2}$ transition.

The emission spectra of the codoped bulk sample as well as the nanocrystalline samples prepared by the two different techniques following excitation with 488 nm are similar in both intensity and peak shape to their respective singly doped erbium Y_2O_3 spectra. Figure 2 presents the NIR emission spectrum of the bulk $Y_2O_3:Er^{3+}$, Yb^{3+} sample and provides evidence that there exists an energy transfer process from the excited Er^{3+} ions to the Yb^{3+} ions in the ground state. Following irradiation of the codoped bulk sample with 488 nm, only the Er^{3+} ions should be excited as Yb^{3+} has only one excited state in the NIR ($\sim$10 600 cm^{-1}) and therefore no emission from the Yb^{3+} ions should be observed. However, we observe peaks attributed to Yb^{3+} emission in the NIR emission spectra and, thus, it is reasonable to assume that an energy transfer between the Er^{3+} and Yb^{3+} ions is operative. The Er^{3+} ion is initially excited to its $^4F_{7/2}$ state with the 488 nm pump photons. A cross-relaxation process of the form $(^4F_{7/2}, {}^2F_{7/2}) \rightarrow (^4I_{11/2}, {}^2F_{5/2})$ occurs following the initial excitation.[19] After the Yb^{3+} ion is excited to its $^2F_{5/2}$ state, it can emit radiatively, as evidenced by the NIR emission spectrum, or it can transfer its energy back to the Er^{3+} ion exciting it to the $^4F_{7/2}$ state once again. It is apparent from the intensity of the $^4S_{3/2} \rightarrow {}^4I_{15/2}$ transition compared to that of the $^4I_{11/2} \rightarrow {}^4I_{15/2}$ and $^2F_{5/2} \rightarrow {}^2F_{7/2}$ transitions, that the back transfer from Yb^{3+} to Er^{3+} is favored over the radiative $^2F_{5/2} \rightarrow {}^2F_{7/2}$ emission from the Yb^{3+} ion. We should note, however, that the peaks attributed to Yb^{3+} emission are very weak and barely detected in the nanocrystalline codoped samples.

The next logical question that must be posed is why this energy transfer does not occur as efficiently in the nanocrystalline material. We believe that this is simply due to the high phonon energies inherent in this type of material. It is known that the nanocrystalline Y_2O_3 powders tend to adsorb H_2O and CO_2 from the atmosphere following synthesis.[3] In fact, vibrational spectra have shown that the present samples contain hydroxyl and carbonate groups, which are located on the nanocrystalline surface.[8] The presence of these groups on the nanocrystalline surface yields higher energy vibrational quanta

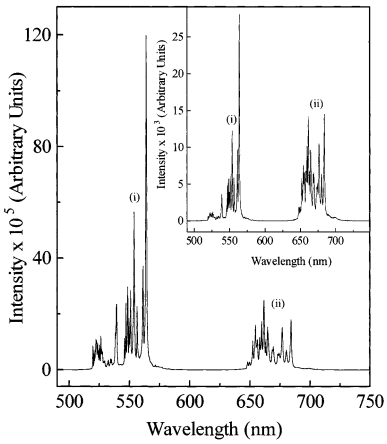

Figure 4. Room temperature anti-Stokes luminescence of bulk Y_2O_3:Er^{3+}, Yb^{3+} following excitation with 978 nm. Inset: room temperature anti-Stokes luminescence of bulk Y_2O_3:Er^{3+}, Yb^{3+} following excitation with 1064 nm: (i) $^2H_{11/2}$, $^4S_{3/2} \rightarrow {}^4I_{15/2}$; (ii) $^4F_{9/2} \rightarrow {}^4I_{15/2}$.

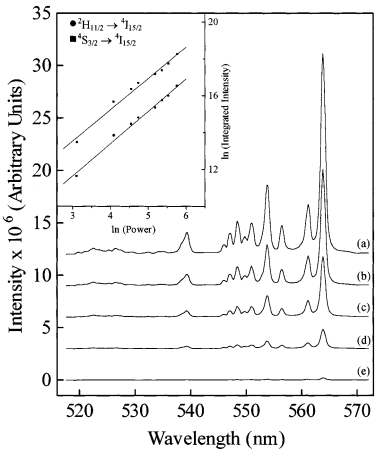

Figure 5. Study of the anti-Stokes luminescence of the $^2H_{11/2}$, $^4S_{3/2} \rightarrow {}^4I_{15/2}$ transitions in bulk Y_2O_3:Er^{3+}, Yb^{3+} following excitation with 978 nm as a function of pump power: (a) 320 mW; (b) 215 mW; (c) 115 mW; (d) 60 mW; (e) 25 mW. Inset: power dependence of the $^2H_{11/2}$, $^4S_{3/2} \rightarrow {}^4I_{15/2}$ anti-Stokes luminescence intensity of bulk Y_2O_3:Er^{3+}, Yb^{3+} observed following 978 nm excitation

as compared to the phonons of bulk yttria (phonon cutoff of about 600 cm^{-1}) and makes multiphonon relaxation much more probable than in the bulk sample. This is evidenced in the luminescence intensity difference between the bulk and the nanocrystalline samples, which had significantly lower overall intensities compared to the bulk material. Thus, these high-energy vibrations reduce many of the radiative processes, allowing the ion to decay primarily via the emission of phonons. In the nanocrystalline material the energy transfer from Er^{3+} to Yb^{3+} is severely limited due to the very efficient multiphonon relaxation from the $^4I_{11/2}$ to the $^4I_{13/2}$ excited state. The high phonon energies significantly reduce the population reservoir in the $^4I_{11/2}$ state, and because this mechanism involves this state, the process becomes highly inefficient.

The residual nitrate ions formed during the combustion process are decomposed after firing the nanocrystals at 500 °C for 1 h; however, this heat treatment was not sufficient enough to remove either the carbonate or hydroxyl ions from the nanocrystal surface. In a previous paper,[8] we showed the MIR spectra obtained after successive heat treatments of Y_2O_3:Er^{3+} nanocrystals where they were heated at 800 °C for 17 h, subsequently cooled to room temperature, and then further treated at 1000 °C for 65 h. Following this heat treatment, the bands occurring at approximately 1500 and 3350 cm^{-1} ascribed to vibrations from the CO_3^{2-} and OH^- groups, respectively, were still observed. However, after the second heat treatment, the overall intensities of the bands at 1500 and 3350 cm^{-1} indicated that the heat treatments reduced the overall surface contamination but, under these experimental conditions, the contaminants were not completely removed. Longer heat treatments at higher temperatures were ruled out because aggregation of the nanoparticles can occur, a process in which they combine to form larger particles. This would make a comparison between the luminescence of the heat-treated and nonheat treated nanocrystalline materials difficult, as the spectroscopy of the nanocrystalline material is particle size dependent.

Anti-Stokes Luminescence. Figures 3 and 4 present the anti-Stokes spectra of nanocrystalline and bulk Y_2O_3:Er^{3+}, Yb^{3+} following excitation with 978 nm radiation. The spectra exhibitthree distinct emission bands centered at approximately 530, 560, and 670 nm and correspond to green emission from the $^2H_{11/2}$, $^4S_{3/2}$ and red emission from the $^4F_{9/2}$ excited states to the $^4I_{15/2}$ ground state of the erbium ions, respectively.

To better understand the mechanism by which the $^2H_{11/2}$, $^4S_{3/2}$, and $^4F_{9/2}$ excited states are populated following NIR irradiation, the upconverted luminescence intensity of the green ($^2H_{11/2}$, $^4S_{3/2} \rightarrow {}^4I_{15/2}$) and red ($^4F_{9/2} \rightarrow {}^4I_{15/2}$) emissions were measured as a function of the excitation power (Figure 5). For any upconversion mechanism, the visible output intensity (I_v) will be proportional to some power (n) of the infrared excitation intensity (I_{IR}):[20,21]

$$I_v \propto I_{IR}^{\,n}$$

where n is the number of IR photons absorbed per visible photon emitted. The graph of $\ln(I_v)$ versus $\ln(I_{IR})$ yields a slope of n equal to approximately 2 for all samples under investigation (Figure 5, inset). Thus, we can propose that two photons are involved in the upconversion mechanism responsible for populating the green and red levels. Following 978 nm irradiation of Y_2O_3, the Er^{3+} ion is excited to the $^4F_{7/2}$ state via two successive energy transfers from the Yb^{3+} ions in the $^2F_{5/2}$ state.[22,23] Thus, one Yb^{3+} ion will transfer its energy to an Er^{3+} ion in the ground state, thereby exciting it to the $^4I_{11/2}$ state. This process is followed by a transfer of energy from another Yb^{3+} ion also in its excited state, resulting in the population of the $^4F_{7/2}$ state of the erbium ion. The lower emitting levels are then populated via multiphonon relaxation and green and red emission is then observed. Of course, interactions between two Er^{3+} ions cannot necessarily be ignored. An NIR photon from the pump beam will also excite an Er^{3+} ion to its $^4I_{11/2}$ state. Another Er^{3+} ion also in the $^4I_{11/2}$ state and in close proximity will transfer its energy to the initial ion, thereby exciting it to the $^4F_{7/2}$ state. However, following the addition of Yb^{3+} ions, this process is greatly diminished due to the large absorption cross-section of the ytterbium ions. Thus, the simultaneous transfer of energy from Yb^{3+}, which populates the $^4F_{7/2}$ state is dominant.

Having described the upconversion pumping mechanisms responsible for populating the $^4F_{7/2}$ state of Er^{3+}, we would expect the green emission to dominate the spectrum, as was the case when directly exciting the $^4F_{7/2}$ state with 488 nm radiation. In the bulk material the green emission still dominates; however, there is a clear difference in the relative green-to-red emission intensity in the upconversion spectrum. In the nanocrystalline material, we observe that this effect is much more pronounced and the red emission in fact dominates the spectrum. This is rather unexpected, as the $^4F_{9/2}$ state is populated via

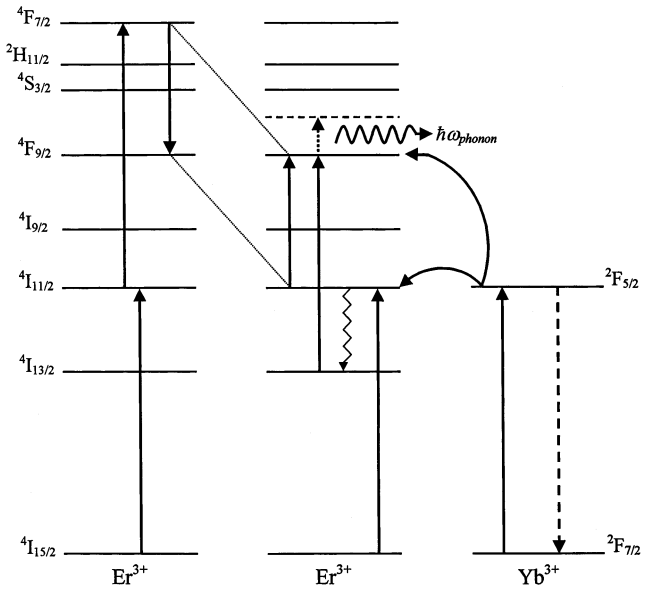

Figure 6. Schematic representation of the ($^4F_{7/2}$, $^4I_{11/2}$) → ($^4F_{9/2}$, $^4F_{9/2}$) ion-pair process responsible for populating the $^4F_{9/2}$ state in $Y_2O_3:Er^{3+}$, Yb^{3+} following 978 nm excitation and of the phonon-assisted energy transfer process responsible for populating the $^4F_{9/2}$ state in $Y_2O_3:Er^{3+}$, Yb^{3+}.

nonradiative decay from the $^4S_{3/2}$ state involving the emission of several phonons to bridge the 3000 cm^{-1} energy gap between the $^4S_{3/2}$ and $^4F_{9/2}$ states. Thus, we would expect the population in the $^4F_{9/2}$ state to be lower than the $^4S_{3/2}$ state as in the bulk material. Therefore, a process must be operative that allows for the bypassing of the $^2H_{11/2}$ and $^4S_{3/2}$ levels while transferring the pump energy to the $^4F_{9/2}$ state.

It is known that microcrystalline $Y_2O_3:Er^{3+}$, Yb^{3+} shows predominantly red emission following infrared excitation with 980 nm[24] into the $^2F_{5/2}$ state of the Yb^{3+} ion in contrast with the direct excitation of the $^4F_{7/2}$ state of Er^{3+} (with 488 nm), which shows predominantly green emission. The enhancement of the population in the red ($^4F_{9/2}$) emitting level was observed to occur through an ion-pair process and is achieved via two resonant transitions: ($^4F_{7/2}$, $^4I_{11/2}$) → ($^4F_{9/2}$, $^4F_{9/2}$) (Figure 6). An enhancement of the red emission occurs in both the bulk and the nanocrystalline samples, albeit to different extents; however as the above process occurs via two energy transfer processes, it should in principle occur with equal probability in both the bulk and the nanocrystalline samples having the same dopant concentration. Thus, this process does not account for such a drastic difference in the magnitude of the red enhancement between the bulk and nanocrystalline samples.

To effectively understand why this phenomenon occurs in the nanocrystalline material and not in the bulk, the structural properties of the samples under investigation must certainly be discussed. The two synthesis techniques produce nanopowders with fundamentally different morphologies. The propellant synthesis gives rise to very porous nanosized materials with a spongelike microstructure directly suggesting a fractal behavior. The building units of this porous structure are composed of crystallites with different orientations and dimensions. These samples show a similar morphology over a large range of magnifications (SEM), which is due to their fractal structure.[15] In contrast, the wet synthesis gives rise to compact nanosized materials with no fractal dimensions. The powders are built up of crystalline platelets with a porous structure at the nanometer scale, which forms large partially ordered aggregates at the micrometer scale.[14] Although the morphologies of the two nanopowders are quite different, the red enhancement occurs in both materials, albeit to a slightly different extent. Therefore, it appears that the microstructure plays only a minor role in this process. As previously discussed, the nanocrystalline lattices contain CO_3^{2-} and OH^- impurities on their surface and thus have available large vibrational quanta to efficiently depopulate the excited states nonradiatively. Thus, this is the distinguishing factor between the bulk and nanocrystalline samples as the bulk lattice does not possess any high-energy phonons and must solely rely on the intrinsic phonons of yttria. Therefore, a mechanism must be operative that utilizes these high-energy phonons.

In the nanocrystalline material, the Er^{3+} ion will decay nonradiatively from the $^4I_{11/2}$ state to the $^4I_{13/2}$ state following the initial energy transfer from the Yb^{3+} ion by very efficient multiphonon relaxation. Essentially, the rate of multiphonon relaxation is dependent upon the energy gap separating the emitting level and the next lower level as well as the highest phonon energy in the material.[25] As the nanocrystalline material possesses relatively high phonon energies, the rate of multiphonon relaxation is rather large. The gap between the $^4I_{11/2}$ and $^4I_{13/2}$ states is approximately 3600 cm^{-1} and few high-energy phonons can easily bridge the gap. In contrast, the bulk material utilizing only the intrinsic yttria phonons to bridge the same gap requires many more phonons. Following the multiphonon relaxation to the $^4I_{13/2}$ state, another energy transfer from the Yb^{3+} ion in the $^2F_{5/2}$ state will excite the Er^{3+} ion to the $^4F_{9/2}$ state.[26,27] However, an excess energy of approximately 1600 cm^{-1} is present and must be dissipated by the lattice to conserve energy (Figure 6). Again, the high phonon energies in the nanocrystalline material can easily accommodate the extra energy.

Further proof for this mechanism is provided from the anti-Stokes emission spectrum of bulk $Y_2O_3:Er^{3+}$, Yb^{3+} following excitation with 1064 nm (Figure 4, inset). The red ($^4F_{9/2}$ → $^4I_{15/2}$) emission was observed to be more intense relative to the green ($^2H_{11/2}$, $^4S_{3/2}$ → $^4I_{15/2}$) emission when compared to the spectrum obtained following excitation with 978 nm. The enhancement in the bulk occurs because the $^4F_{9/2}$ ← $^4I_{13/2}$ transition is nearly resonant with the 1064 nm line of the Nd:YAG laser.[27] The excess energy in this transition is on the order of about 800 cm^{-1} and thus the probability of the process occurring in the bulk material is much greater, resulting in an enhancement of the $^4F_{9/2}$ population. Shionoya[10] showed from experimental evidence that the phonon of ~400 cm^{-1} and not the maximum phonon energy contributes dominantly to the energy transfer processes and therefore is more coupled to the electronic transitions. Thus, the bulk sample would require only two yttria phonons to conserve energy in the process.

The natural extension of this work is to study the concentration and temporal effects on the upconversion in bulk and nanocrystalline $Y_2O_3:Er^{3+}$, Yb^{3+}. Studies in this direction have been initiated and will be the subject of a future paper.

Conclusions

Following direct population of the $^4F_{7/2}$ excited state with 488 nm of nanocrystalline and bulk $Y_2O_3:Er^{3+}$, Yb^{3+}, we observe a visually dominant green emission ascribed to the $^2H_{11/2}$, $^4S_{3/2}$ → $^4I_{15/2}$ transition as well as red emission from the $^4F_{9/2}$ → $^4I_{15/2}$ transition. NIR emission following 488 nm excitation shows bands attributed to emission from the $^2F_{5/2}$ → $^2F_{7/2}$ transition of Yb^{3+} and indicates that transfer of energy from Er^{3+} to Yb^{3+} is present. Excitation of the samples with 978 nm populates the $^4F_{7/2}$ state via two successive energy

transfers from the Yb^{3+} ions and yields intense anti-Stokes green and red luminescence. We observed an enhancement of the red emission in both the nanocrystalline and bulk material. However, the magnitude of the red enhancement was much more pronounced in the nanocrystalline material. The Er^{3+} ion-pair process of the form ($^4F_{7/2}$, $^4I_{11/2}$) → ($^4F_{9/2}$, $^4F_{9/2}$), which can populate the $^4F_{9/2}$ state, however, does not account for the drastic differences in the red enhancement between the bulk and nanocrystalline samples. A fundamental difference between the bulk and nanocrystalline material is the presence of large vibrational quanta of about 1500 and 3300 cm^{-1} due to ions on the nanocrystalline surface, from adsorbed CO_2 and H_2O, respectively. It was determined that a phonon-assisted energy transfer process occurs more readily in the nanocrystalline samples due to an enhanced multiphonon relaxation from the $^4I_{11/2}$ excite state to the $^4I_{13/2}$ state because of the presence of these vibrational quanta. A subsequent energy transfer from a Yb^{3+} ion will excite the Er^{3+} ion to the $^4F_{9/2}$ state with the high-energy phonons easily dissipating the excess energy via lattice vibrations.

Acknowledgment. We gratefully thank Erica Viviani (Università di Verona, Italy) for expert technical assistance and Stefano Polizzi (Università di Venezia, Italy) for the X-ray measurements on nanocrystalline $Y_2O_3:Er^{3+}$, Yb^{3+}. We acknowledge the Natural Science and Engineering Research Council of Canada and MURST (project 9903222581_005) of Italy, for financial support.

References and Notes

(1) Eilers, H.; Tissue, B. M. *Chem. Phys. Lett.* **1996**, *251*, 74−78.
(2) Bhargava, R. N. *J. Lumin.* **1997**, *72*−*74*, 46−48.
(3) Capobianco, J. A.; Vetrone, F.; D'Alesio, T.; Tessari, G.; Speghini, A.; Bettinelli, M. *Phys. Chem. Chem. Phys.* **2000**, *2*, 3203−3207.
(4) Zych, E.; Hreniak, D.; Strek, W. *J. Phys. Chem. B* **2002**, *106*, 3805−3812.
(5) Goldburt, E. T.; Kulkarni, B.; Bhargava, R. N.; Taylor, J.; Libera, M. *J. Lumin.* **1997**, *72*−*74*, 190−192.
(6) Williams, D. K.; Yuan, H.; Tissue, B. M. *J. Lumin.* **1999**, *83*−*84*, 297−300.
(7) Goldner, P.; Pellé, F. *J. Lumin.* **1994**, *60&61*, 651−654.
(8) Capobianco, J. A.; Vetrone, F.; Boyer, J. C.; Speghini, A.; Bettinelli, M. *J. Phys. Chem. B* **2002**, *106*, 1181−1187.
(9) Cantelar, E.; Sanz-García, J. A.; Cussó, F. *J. Cryst. Growth* **1999**, *205*, 196−201.
(10) Yamada, N.; Shionoya, S.; Kushida, T. *J. Phys. Soc. Jpn.* **1972**, *32*, 1577−1586.
(11) Ye, T.; Guiwen, Z.; Weiping, Z.; Shangda, X. *Mater. Res. Bull.* **1997**, *32*, 501−506.
(12) Tessari, G.; Bettinelli, M.; Speghini, A.; Ajò, D.; Pozza, G.; Depero, L. E.; Allieri, B.; Sangaletti, L. *Appl. Surf. Sci.* **1999**, *144*−*145*, 686−689.
(13) Sharma, P. K.; Nass, R.; Schmidt, H. *Opt. Mater.* **1998**, *10*, 161−169.
(14) Polizzi, S.; Battagliarin, M.; Bettinelli, M.; Speghini, A.; Fagherazzi, G. *J. Mater. Chem.* **2002**, *12*, 742−747.
(15) Polizzi, S.; Fagherazzi, G.; Battagliarin, M.; Bettinelli, M.; Speghini, A. *J. Mater. Res.* **2001**, *16*, 146−154.
(16) Saiki, A.; Ishizawa, N.; Mizutani, N.; Kato, M. *J. Ceram. Soc. Jpn.* **1985**, *93*, 649−654.
(17) Wyckoff, R. W. G. *Crystal Structures*; 2nd ed.; Interscience: New York, 1964; Vol. 2.
(18) Forest, H.; Ban, G. *J. Electrochem. Soc.* **1969**, *116*, 474−478.
(19) de Sousa, D. F.; Zonetti, L. F. C.; Bell, M. J. V.; Lebullenger, R.; Hernandes, A. C.; Nunes, L. A. O. *J. Appl. Phys.* **1999**, *85*, 2502−2507.
(20) Pollnau, M.; Gamelin, D. R.; Lüthi, S. R.; Güdel, H. U.; Hehlen, M. P. *Phys. Rev. B* **2000**, *61*, 3337−3346.
(21) Chamarro, M. A.; Cases, R. *J. Lumin.* **1990**, *46*, 59−65.
(22) Auzel, F. *C. R. Acad. Sci. (Paris)* **1966**, *262*, 1016−1019.
(23) Johnson, L. F.; Guggenheim, H. G.; Rich, T. C.; Ostermayer, F. W. *J. Appl. Phys.* **1972**, *43*, 1125−1137.
(24) Wittke, J. P.; Ladany, I.; Yocom, P. N. *J. Appl. Phys.* **1972**, *43*, 595−600.
(25) Riseberg, L. A.; Moos, H. W. *Phys. Rev.* **1968**, *174*, 429−438.
(26) Kuroda, H.; Shionoya, S.; Kushida, T. *J. Phys. Soc. Jpn.* **1972**, *33*, 125−141.
(27) Page, R. H.; Schaffers, K. I.; Waide, P. A.; Tassano, J. B.; Payne, S. A.; Krupke, W. F. *J. Opt. Soc. Am. B* **1998**, *15*, 996−1008.